

# NU-AIR - A Neuromorphic Urban Aerial Dataset for Detection and Localization of Pedestrians and Vehicles

Craig Iaboni<sup>1,2</sup>, Thomas Kelly<sup>2,3</sup>, Pramod Abichandani<sup>1,2\*</sup>

<sup>1</sup>Department of Computer Science, New Jersey Institute of Technology, 323 Martin Luther King Jr. Blvd, Newark, 07102, NJ, USA.

<sup>2</sup>Electrical and Computer Engineering Department, New Jersey Institute of Technology, 323 Martin Luther King Jr. Blvd, Newark, 07102, NJ, USA.

<sup>3</sup>School of Applied Engineering and Technology (SAET), New Jersey Institute of Technology, 323 Martin Luther King Jr. Blvd, Newark, 07102, NJ, USA.

\*Corresponding author(s). E-mail(s): [pva23@njit.edu](mailto:pva23@njit.edu);  
Contributing authors: [csi3@njit.edu](mailto:csi3@njit.edu); [tjk39@njit.edu](mailto:tjk39@njit.edu);

## Abstract

This paper presents an open-source aerial neuromorphic dataset that captures pedestrians and vehicles moving in an urban environment. The dataset, titled NU-AIR, features 70.75 minutes of event footage acquired with a  $640 \times 480$  resolution neuromorphic sensor mounted on a quadrotor operating in an urban environment. Crowds of pedestrians, different types of vehicles, and street scenes featuring busy urban environments are captured at different elevations and illumination conditions. Manual bounding box annotations of vehicles and pedestrians contained in the recordings are provided at a frequency of 30 Hz, yielding 93,204 labels in total. Evaluation of the dataset's fidelity is performed through comprehensive ablation study for three Spiking Neural Networks (SNNs) and training ten Deep Neural Networks (DNNs) to validate the quality and reliability of both the dataset and corresponding annotations. All data and Python code to voxelize the data and subsequently train SNNs/DNNs has been open-sourced.

**Keywords:** Computer vision, event cameras, spiking neural networks, dataset, UAVs

## 1 Introduction

Traditional cameras operate by sampling the field of view at fixed intervals, producing a series of discrete frames that represent static snapshots of the environment. Event cameras differ from traditional ones in that they record asynchronous events rather than continuous frames [33]. An event is a change in pixel illumination intensity and consists of the pixel's position  $(x, y)$ , the timestamp  $t$  of the illumination change, and the

polarity  $p$  indicating that the illumination intensity increased ( $p = 1$ ) or decreased ( $p = 0$ ). Event cameras have higher temporal resolution, dynamic range and power efficiency compared to traditional frame-based cameras, making them popular for applications in autonomous vehicles, and robotics/IoT systems where low latency and robustness to lighting conditions important [82].

Spiking Neural Networks (SNNs) are inspired by the discrete and asynchronous nature of biological neuron communication. Their compatibility

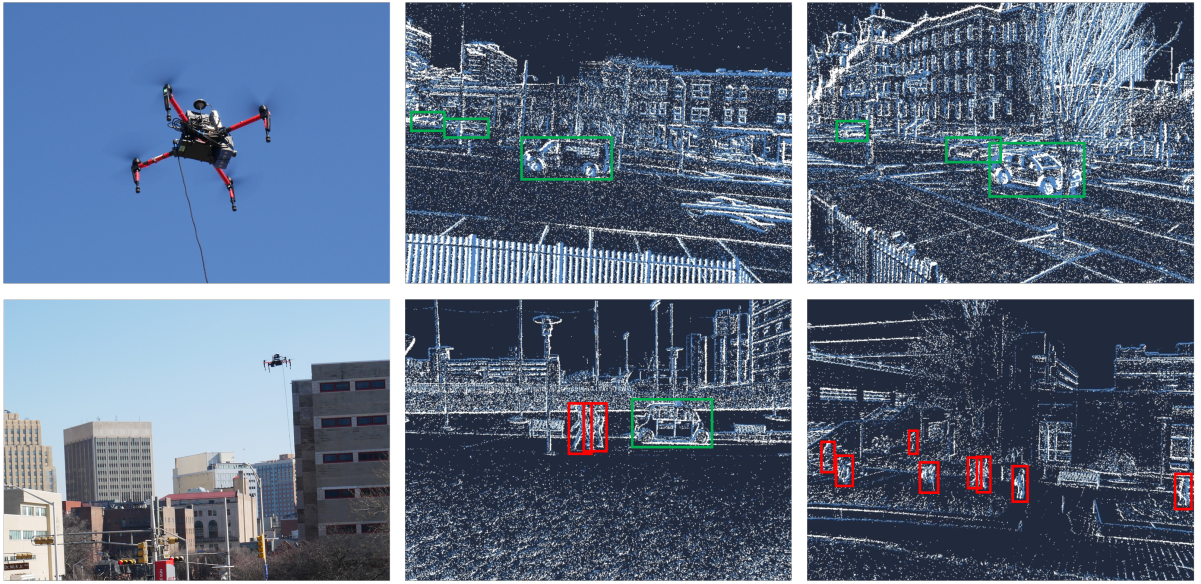


**Fig. 1** (Left Top and Bottom) The DJI M-100 quadrotor was used to record pedestrians and vehicles in urban environments. A safety rope was affixed to the quadrotor during all flight operations. The recording quadrotor flew at varying heights above a city intersection (Top Mid and Right), a walking path (Bottom Mid), and a campus center (Bottom Right). Bounding boxes created by manual annotators were drawn over frames.

with event-based data makes them particularly suited for processing information from event cameras. SNNs are being increasingly used for tasks such as object detection, motion tracking, and sensor fusion in conjunction with event cameras [52, 28].

Large-scale datasets are crucial for developing robust and effective computer vision algorithms. Event cameras are relatively expensive compared to RGB cameras, making it challenging for researchers and practitioners to access them. The availability of neuromorphic datasets is relatively low [80, 101, 67, 46, 47, 14, 2], and only a handful of them feature urban settings [70, 64, 96, 20, 77], with none of the existing neuromorphic urban datasets providing aerial footage leaving a gap in the neuromorphic dataset landscape.

As depicted in Figure 1, this study addresses this gap by introducing a neuromorphic dataset consisting of event-recording segments captured from a quadrotor-mounted event camera observing an urban environment during both daytime and nighttime settings. The dataset is fully annotated, enabling the development and evaluation of new event-based vision algorithms for urban settings.

The main contribution of this study is the open source Neuromorphic Urban Aerial (NU-Air)

dataset that aims to advance the study of neuromorphic vision algorithms design. The dataset is uniquely comprised of 70.75 minutes of quadrotor-mounted event camera recordings, segmented into 283 clips of 15 seconds each. These recordings span diverse environment variations including a university campus, traffic intersections, and walking paths in both daytime and nighttime settings. The NU-AIR Dataset has been meticulously annotated for two crucial classes of detection, namely persons and vehicles, with a total of 93,204 annotations in the form of upright rectangular bounding boxes and corresponding class labels. Figure 1 illustrates examples from this dataset, along with the quadrotor platform used in the data collection.

Beyond the creation of this dataset, this work also involved a comprehensive ablation study of existing neuromorphic vision algorithms. Specifically, Visual Geometry Group (VGG) [95], DenseNet [45], and MobileNet [44] SNNs have been trained using the NU-AIR Dataset and their performances have been compared to previous benchmarks on neuromorphic data.

Additionally, the performance of 10 different Deep Neural Networks (DNNs) was evaluated after training them on the NU-AIR Dataset, further broadening the assessment of neuromorphic vision algorithms. The mean average precision

(mAP) was reported for each experiment. The dataset as well as associated Python code to voxelize the dataset and train the SNNs and DNNs has been made publicly available through the following repository link: <https://bit.ly/nuair-data>

While the unique attributes of the proposed dataset broaden its applicability across various visual computation paradigms, it becomes imperative to elucidate the central role and inherent complexities of object detection within the scope of neuromorphic vision, especially when benchmarked against existing public datasets. Object detection, notwithstanding its pervasive nature in the domain, stands as both a foundational and arduous task in computer vision [109]. The necessity of accurately distinguishing and categorizing entities within visual scenes, especially against the backdrop of dynamic and intricate environments, holds significance across a spectrum of applications, spanning from industrial automation, cutting-edge surveillance systems, autonomous vehicular guidance, to precise ecological monitoring, among others [42, 66, 81, 107, 87, 83, 21, 88, 100, 32, 43].

## 2 Related Works

A number of datasets in the literature have reported on pedestrian and vehicle detection in urban environments.

### 2.1 Frame-based Urban Datasets

Traditional frame-based cameras for object detection of real-world urban scenes have been used to create several pedestrian detection datasets for training and evaluation purposes, including ETH [29], INRIA [19], PRW [106], TUD-Brussels [104], and Daimler [27]. Larger and more diverse collections such as KITTI [34], Caltech-USA [24], UA-DETRAC [103], CityPersons [105], EuroCity Persons [10], TRANCOS [39], and TJU-DHD [75] have allowed researchers and practitioners to push the limits of algorithmic performance at scale. These sets were recorded by driving or walking through urban areas and provide annotated frames from video sequences.

Drone-mounted RGB cameras have been utilized to generate multiple real-world aerial datasets. The Urban Drone Dataset (UDD) [15] features diverse urban scenes from 10 video

sequences captured in 4 cities in China. It includes semantic annotations for 6 detection classes and comprises of 160 training and 45 validation images. The UAV123 [68] dataset includes 123 aerial video sequences, with bounding box annotations provided for every sequence. The VizDrone [108] dataset has 288 video clips and 10,209 static images captured from drone-mounted cameras, manually annotated with over 2.6 million bounding boxes. The OpenDD [11] dataset covers seven roundabouts in Germany, including over 80,000 road bounding boxes in 62+ hours of data. The UAVDT [26] dataset includes 100 video sequences with approximately 80,000 representative frames, captured at various urban locations such as highways and crossings.

### 2.2 Event-based Camera Datasets

Early event-based datasets have been created by converting frame-based datasets to event format for benchmarking tasks [73, 92, 31, 57]. The benefit of these methods is that large datasets can be generated without manual labeling. However, the low screen refresh rate of displays create unnatural event sequences. As a result, recent efforts have centered on creating real-world datasets for detection and recognition of persons, animals, objects, robots, and quadrotors [2, 14, 101, 80, 67, 46, 47]. The majority of these event-based datasets have been collected in controlled, indoor environments.

#### 2.2.1 Real-World Urban Event Datasets

The following discussions highlight the fact that only a handful of studies have provided open-source image/video datasets capturing urban settings [70, 64, 96, 20, 77].

- The Scenes-DVS [70] set consists of recordings of long hikes in urban environments, with sequences of indoor and outdoor environments exceeding 15 minutes long split into small 50ms sequences. Scene classification accuracy was evaluated with a frame based single-layer and three multi-layer SNN configurations (with varying hidden layer sizes) [71]. The highest accuracy reported for the single-layer architecture and multi-layer architecture was 81.2% and 84.4%, respectively.

- The PAFBenchmark pedestrian detection dataset [64] contains 4670 frame images at 20ms time intervals with bounding box annotations of scenarios seen in traffic surveillance tasks such as pedestrian overlapping, occlusion, and collision.
- N-Cars [96] is a large, real-world event-based dataset for car classification. It is composed of 12,336 car samples and 11,693 non-car samples (background). Each sample lasts 100ms. Classification accuracy for the two-class problem was evaluated using a linear SVM classifier. 90% classification accuracy was reported for this evaluation.
- The Gen1 Automotive [20] contains 39 hours of open road and various driving scenarios ranging from urban, highway, suburbs, and countryside scenes. Manual bounding box annotations are provided for two classes of detection: pedestrian and cars. The capture resolution of this set is  $304 \times 240$ . The data has not been evaluated for classification or detection accuracy in this study.
- The 1 Megapixel Automotive [77] dataset includes 14 hours of annotated vehicles and pedestrians captured within roadway scenes. This set is the highest resolution neuromorphic object detection dataset from a vehicle-mounted perspective to date, with a capture resolution of  $1280 \times 1024$ . A recurrent ConvLSTM architecture is used to evaluate the proposed dataset [94]. A mAP of 0.43 was reported for automotive detection using the proposed architecture.

### 2.3 NU-AIR Versus Other Datasets

The proposed NU-AIR dataset represents a significant advancement over previously reported datasets by offering several distinct characteristics. Contrasting with existing benchmarks, NU-AIR capitalizes on the high temporal resolution of neuromorphic sensors, gathering data via cameras mounted on quadrotors navigating intricate urban topologies. This configuration inherently yields high-dimensional scene variations, encapsulating temporal dynamics and urban microstructures, resulting in a dataset that is both granular and temporally rich [40]. Unconstrained by terrestrial limitations, drones maneuver seamlessly over intricate and demanding terrains, sidestepping challenges endemic to vehicle-based systems [18, 9].

Their ability to hover at varied altitudes and unrestricted yaw, pitch, and roll orientations allows for a dataset which meticulously captures the geometric and radiometric intricacies of the surveyed environments from diverse optical perspectives [63, 51]. Conversely, vehicle-affixed imaging modalities, bound to their terrestrial constraints, primarily capture data through a restricted lateral optical aperture [53]. Such a perspective is inherently prone to occlusions, generated by terrain variations and physical obstacles [3, 79, 13]. The outcome is data that may be riddled with occlusion gaps and potential distortions, particularly when documenting elevated structures or expansive regions [7]. This stark distinction underscores the significant advantages that drones present in the landscape of spatial data acquisition [58, 85].

Anchoring the dataset is the integration of precise bounding box annotations, optimized for a multi-class detection framework. These annotations provide a structured ground truth that enables algorithmic training, thus facilitating high-precision performance metrics and evaluation benchmarks. By embracing the event-driven, sparse, asynchronous nature intrinsic to neuromorphic cameras, the dataset brings forth a myriad of challenges—ranging from handling high temporal discrepancies, mitigating drone-induced perturbations such as motion blur, to addressing complex visual phenomena like parallax and rapid perspectival alterations.

NU-AIR’s heterogeneity is enhanced by diverse illumination conditions and varied environmental scenarios, including university campuses, pedestrian-centric walkways, and dynamic traffic intersections. This diversity serves as a robust platform for advancing event-driven vision algorithms, necessitating the exploration of adaptive thresholding, noise filtering, and temporal clustering techniques to each unique stimulus.

The remainder of this paper is organized as follows. In Section 3, the recording setup, annotation procedure, and dataset format are discussed. In Section 4, the use of SNNs and DNNs to benchmark the performance of the proposed dataset is described. Additionally, a detailed ablation study has been performed to further investigate the contribution of various components to the overall SNN performance. In Section 5, a detailed discussion of the potential limitations and constraints encountered during the study is provided. Section

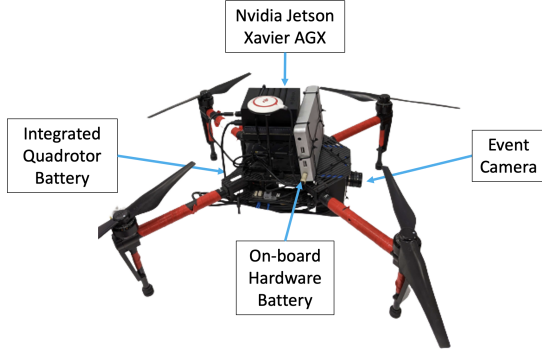


**Fig. 2** The DJI Matrice M100 quadrotor with a forward-facing Propesee Gen3.1 VGA event camera was used for data collection.

6 summarizes the paper, emphasizing key findings and outlining future directions.

### 3 Dataset

This section explains how the NU-AIR dataset was collected (subsection 3.1), the annotation process (subsection 3.2), the file structure (subsection 3.3), and the Voxel Cube encoding format (subsection 3.4).

#### 3.1 Recording Setup

This study used a Propesee Gen3.1 VGA ( $640 \times 480$ ) resolution event camera [78]. This camera operates on 1.8 V supplied via USB, with a 10 mW power dissipation rating in low-power mode. The brightness intensity measurements from the sensor were used to create gray-scale frames at a frequency of 30 Hz, which were then manually annotated by human subjects to generate ground-truth bounding boxes around areas of interest.

As shown in Figure 2, the camera was mounted on a DJI M100 quadrotor with a  $10^\circ$  downward mounting angle [22]. The camera was connected to an on-board NVidia Jetson Xavier AGX computer for data recording via USB [72]. The recording setup and quadrotor were powered by isolated batteries to ensure reliable operations of the entire setup. The Jetson was powered by a 28800 mAh capacity DC 12V power bank, while the quadrotor was equipped with a 5700 mAh capacity TB48D battery [23]. A safety rope, as shown in Figure 1, was attached to the quadrotor for all flight tests.

The data was collected from three different real-world scenes - a crowded university campus

center, a walking path with low foot traffic, and a city intersection with high vehicle traffic in New Jersey, USA. The quadrotor was translated (roll and pitch) and rotated (using yaw control) while collecting the footage. The recordings ranged from one to five minutes in duration and were captured over the course of one week in December, at varying times of the day to include different lighting and weather conditions. A total of 70.75 minutes, split among 14 recordings, were collected, yielding 238GB of raw event data. In comparison, a gray-scale frame-based camera with the same resolution and operating at a frequency of 120fps (i.e. 100 times lower temporal resolution compared to the event camera) would have generated over 359GB of data<sup>1</sup>. Figure 3 depicts several snapshots of the acquired footage.

#### 3.2 Manual Annotation

By using the change detection events provided by the neuromorphic sensor, it is possible to generate gray-scale images at any desired temporal resolution, precisely aligned with the events stream. Such alignment ensures that annotations on the gray-scale images can be applied directly as ground truth for the events stream without requiring calibration or correction, as they share the same pixel array [96].

Given the high temporal resolution of the event camera, gray-scale images were generated at a frequency of 30Hz for annotation. The images were then given to human annotators to draw bounding boxes around pedestrians and vehicles. The traditional method of drawing a bounding box, used in the annotation of datasets such as ILSVRC [86] and introduced by Su et al. [98], involves manually selecting imaginary corners to tightly encase an object. This can be challenging, as the desired corners may fall outside the physical bounds of the object, often necessitating numerous adjustments to achieve an accurate bounding box. For this dataset, we opted to use the extreme clicking technique [76] for all bounding boxes. This method simplifies the task by requiring annotators to identify four physical points on the object: the top, bottom, left-, and right-most points. These tangible points facilitate a more natural task that is

---

<sup>1</sup>Ignoring compression and assuming 1 byte per pixel

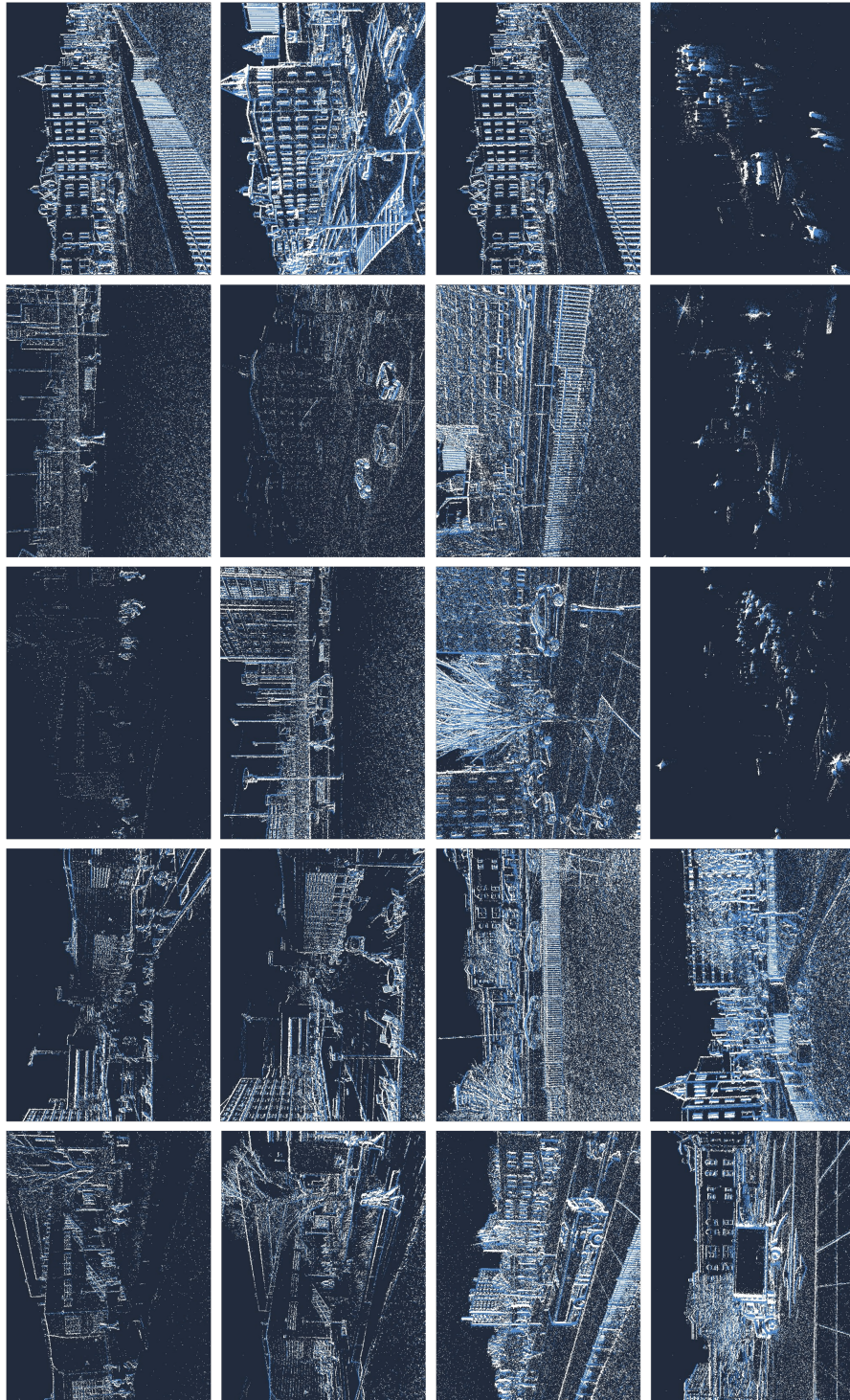


**Fig. 3** Sample images from the NU-AIR dataset showcasing the diversity of urban environments and the intricate challenges presented by drone-based neuromorphic imaging.

more readily performed, thus enhancing both efficiency and precision.

In order to guarantee the quality of our annotation results, a temporally sequential annotation

process was conducted. Specifically, all annotations are inherited from the previous frame and then updated according to object appearances in the current frame. This process can both maintain high temporal consistency in the annotation results and greatly reduce the annotation burden at the same time.

Specific instructions were provided to the annotators to minimize ambiguity and inconsistencies among annotations. Objects smaller than 10 pixels or those partially occluded (less than 50% visible) were disregarded. Various large vehicles, such as cars, buses, and trucks, were annotated uniformly within the vehicle category. Persons within cars or buildings were excluded from annotation. A total of 66958 vehicle and 26246 pedestrians bounding boxes have been annotated using the extreme clicking technique. The annotations produced were reviewed by two experts to ensure location accuracy and subject correctness. Example gray-scale images with manual annotations are shown in Figure 1.

### 3.3 Dataset Format

The dataset was captured across 14 continuous recording sessions. In order to facilitate the training, the continuous recordings were divided into 15 seconds intervals, resulting in a total of 283 samples. The total samples were divided into training, validation, and testing subsets with 197, 57, and 29 samples in each subset, respectively. To avoid overlap between subsets, events from each continuous recording session were assigned to the same subset.

Each sample was provided in a binary .dat format, where events were encoded using 4 bytes for the timestamps and 4 bytes for the position and the polarity. Specifically, 14 bits are used for the  $x$  position, 14 bits for the  $y$  position, and 1 bit for the polarity. Python code to generate gray-scale images from binary files is provided with the dataset.

Bounding box annotations follow a `numpy` format [41]. Each `numpy` array contains the following fields:

- $t_s$ , timestamp of the box in microseconds
- $x$ , abscissa of the top left corner in pixels
- $y$ , ordinate of the top left corner in pixels
- $w$ , width of the box in pixels
- $h$ , height of the box in pixels

- $class_id$ , class of the object: 0 for pedestrians and 1 for vehicles

Python code to load and view samples from the dataset with the corresponding annotations visualized has been provided. Within the released code repository, an example on how to apply the evaluation metrics on the dataset is provided.

### 3.4 Voxel Cube Encoding

Voxel cubes were used to encode event data [17]. This approach offers advantages over event encoding strategies such as event frames, two-channel images, and time surfaces in that events are not collapsed to a 2D grid, thus conserving both binarity and temporal information while allowing for batched processing of events [33]. The voxel cube encoding method is inspired by voxel grid encoding. Voxel grid encoding is an encoding method in which a series of bins are used to convert the temporal dimension to a set of event volumes [6]. A voxel grid is represented by a 3D THW tensor of events, where  $T$  is the number of timesteps, and  $H$  and  $W$  are the height and width of the data respectively [6]. The accumulation of events within the time interval is either a sum [30] or a binary accumulation [16].

In the case of binary accumulation, when events within the represented time interval do not overlap on a particular voxel, the complete set of events can be retrieved from the representation. When multiple events intersect on a voxel, only the most recent event is represented in the voxel. Thus, temporal information describing the frequency of the event occurrence at the given voxel is lost, but the volume still reflects the distribution of events across spatial and temporal dimensions.

By contrast, the voxel cube encoding technique subdivides each event volume into smaller sub-volumes, referred to as voxel cubes. A voxel cube is represented by a 4D CTHW tensor, where  $C$  is the number of channels,  $T$  is the number of timesteps, and  $H$  and  $W$  are the height and width of the data respectively [17]. The events within a sub-volume are assigned to a cell depending on position  $(x,y)$  and to a sub-volume depending on timestamp  $(t)$ . Rather than counting event frequency like a histogram, each event is counted based on its temporal distance from the center of neighboring sub-volumes. The value of each

event is distributed over the two nearest sub-volumes, and weighted by the temporal distance between the event and the centroids of neighboring sub-volumes. In this way, temporal information is preserved as all events that fall within a sub-volume give a varying contribution based on the event timestamp.

## 4 Performance of Baseline DNNs and SNNs

In this section, experiments are provided to quantify the performance of baseline models for object detection on the NU-AIR dataset.

### 4.1 Frame-based DNNs

A total of 10 single-stage or two-stage frame-based object detection DNNs were used in this study and their COCO mean average precision (mAP) metric has been reported. The models include YOLOv5n [50], YOLOv5s [50], YOLOv6n [56], YOLOv6s [56], YOLOv7t [102], YOLOv7 [102], YOLOv8n [49], YOLOv8s [49], Faster-RCNN [84], and RetinaNet [60]. Training was performed on Google Colaboratory with the standard GPU and memory configuration provided by the platform [37]. The evaluation involved selecting the two smallest configurations of each variant of the YOLO object detector network, except for YOLOv7, where the smallest two networks were named YOLOv7-tiny and YOLOv7. The network size selection was made to evaluate the networks' performances on edge devices that compete with low-power neuromorphic hardware. For Faster-RCNN and RetinaNet, only one variant each was evaluated. The number of parameters in each model is reported in millions.

#### 4.1.1 DNN Results

Table 1 depicts the performance of various DNNs for the NU-AIR dataset. From the table, it is evident that YOLOv7 achieved the highest mAP of 0.53, whereas both RetinaNet and YOLOv5n reported an identical mAP of 0.37, which was among the lowest scores.

Despite the general trend observed where larger models like YOLOv7 perform better than smaller models, there are anomalies where smaller models managed to outperform or closely match

**Table 1** The COCO mean average precision (mAP) for 10 object detection models trained on the NU-AIR dataset.

DNN Methods	Params	mAP
YOLOv5n	1.9M	0.37
YOLOv5s	7.2M	0.39
YOLOv6n	4.3M	0.41
YOLOv6s	17.2M	0.39
YOLOv7t	6.2M	0.36
YOLOv7	36.9M	0.53
YOLOv8n	3.2M	0.42
YOLOv8s	11.2M	0.44
Faster-RCNN	19M	0.42
RetinaNet	36.4M	0.37

their larger counterparts. For instance, the relatively smaller YOLOv5s surpassed the performance of the considerably larger RetinaNet. Additionally, the smaller YOLOv6 variant did not follow the expected pattern, and outperformed its larger sibling. This observation, although indicative of the nuances within specific model architectures and their adaptability to the dataset, still aligns with the broader trend in deep learning.

### 4.2 Event-based SNNs

Three SNNs were trained and their performance has been evaluated in terms of accuracy. All SNN models were trained using the Decoupled Weight Decay Regularization (AdamW) optimizer [62], with a weight decay of  $1e^{-4}$ . Each model started with an initial learning rate of  $1e^{-3}$ . The training process, spanning 50 epochs with a batch size of 64, was executed on a Google Cloud Compute instance equipped with NVidia Tesla T4 GPU and 64 GB of memory [38]. A cosine annealing scheduler was used to gradually reduce the learning rate to 0. Convolutions were initialized with the Kaiming uniform method. Batch normalization layers began with a weight of 1 and a bias of 0.

The Parametric Leaky Integrate-and-Fire (PLIF) neurons integrated specific parameters to expand the adaptability and versatility of the network. The PLIF neuron is a spiking neuron with learnable membrane parameters, thus enhancing the expressiveness of the SNN [30]. The time constant of the neuron's membrane potential, represented by the parameter  $\tau$ , was set to a default value of 2, determining the rate at which the potential decays towards its resting state. When the accumulated potential of the neuron reached or surpassed the set threshold of 1, the neuron

emitted a spike. To allow gradient computation during the backward pass, especially given the non-differentiability of the actual spiking function, the ATan (arctangent) function was used as a surrogate, offering a smooth and differentiable approximation. Gradient norms featured an upper-bound of 1 to prevent exploding gradients. The final results were obtained by averaging over three training runs. The SNNs featured the following details:

1. *Spiking VGG* [95]: VGG (Visual Geometry Group) is a CNN that consists of up to 19 convolutional layers, followed by 3 fully-connected layers. The spiking variant of VGG includes batch normalization layers added before each spiking convolutional layer. The VGG SNN in this work featured 11 convolutional layers.
2. *Spiking DenseNet* [45]: DenseNet is an architecture that promotes gradient propagation by using channel-wise concatenations, which is an operation that preserves spike representation. DenseNet configurations are defined by the depth (number of layers within the network) and growth rate (how much new information each layer contributes to the global state). For the spiking variant, ReLU activations are replaced with PLIF. The spiking DenseNet architecture in this work used a depth of 120 convolution layers and 1 fully connected layer with a growth rate of 24.
3. *Spiking MobileNet* [44]: MobileNet is a model intended for use in mobile applications that use depth-wise separable convolutions which need fewer parameters and computations compared to traditional convolutions. By varying the number of input channels, MobileNet can be evaluated at various sizes. The spiking version of MobileNet removes the activation function between the depth-wise and point-wise convolutions, and positions all batch normalization layers before the convolutional layers. The spiking MobileNet in this work used 16 input channels.

The SNNs are combined with Single Shot MultiBox Detector (SSD) bounding box regression heads to perform object detection. The SSD object detection framework consists of a spiking classifier backbone and multiple predictor heads [61]. The heads take feature maps generated by the classifier at different scales as input, and outputs bounding

boxes with associated classes. Readers are referred to [17] for further implementation details about the SNNs used for the analysis presented here.

For the task of object detection, the mAP over 10 IoU ([0.5:0.05:0.95] – the COCO mAP) is reported [59]. However, assessing the performance of SNNs is not limited to mAP, as multiple others features are needed to take advantage of their benefits when embedded in specialized hardware. For all results, the following metrics are reported in Table 2:

- *Number of parameters*: To meet the high memory constraints of embedded systems, the network size is measured in terms of the number of parameters.
- *Number of accumulation operations (ACCs)* : SNNs do not require multiplicative operations, enabling substantial energy savings on specialized hardware. The number of accumulation operations (ACCs) is reported to highlight potential energy savings. All spiking convolution operations amount to ACCs, and each PLIF neuron only requires 1 ACC per timestep to update its potential. Batch normalization layers are not included in the ACCs count.
- *Sparsity*: The number of spikes emitted after each activation layer were measured to represent the global sparsity of the network compared to an fully dense equivalent Deep Neural Network (DNN). Processing events with SNNs preserves the data sparsity [54]. On specialized hardware, computations are only performed when there are spikes, therefore a highly sparse network would consume less power than its dense counterpart. The sparsity is obtained by averaging the number of spikes over the whole test set.

**Table 2** Comparison of three tested SNN configurations detailing network size in millions of parameters, number of accumulations per timestep, and network sparsity.

SNN Methods	Params	ACC/ts	Sparsity	mAP
VGG-11 + SSD	12.6M	11.1G	23.1%	0.17
DenseNet121- 16 + SSD	8.2M	2.3G	38.1%	0.17
MobileNet- 16 + SSD	24.3M	4.3G	27.9%	0.13

#### 4.2.1 SNN Results

For SNN object detection models, three configurations of classifier and SSD network are used for evaluation. The COCO mAP accuracy results of the three SNNs trained on this dataset are given in Table 2.

- The VGG-11 + SSD network configuration achieved a COCO mAP of 0.17, which is tied with DenseNet121-16 + SSD for the highest evaluation metric observed in this work. The size of this network configuration was 12.6M parameters, with 11.1B accumulation operations per timestep, and a sparsity of 23.1%.
- The DenseNet121-16 + SSD network configuration achieved a COCO mAP of 0.17. The network contained 8.2M parameters. The number of accumulation operations per timestamp for this network was the least among the evaluated SNNs at 2.3B. At 38.1% sparsity, this network was the most dense of the evaluated SNNs.
- The MobileNet-16 + SSD network configuration achieved a COCO mAP of 0.13. This was the lowest reported mAP result among the three SNNs used for dataset evaluation. This network configuration was the largest of the evaluation SNNs at 24.3M parameters. This network performed 4.3B accumulation operations per timestep, with a sparsity of 27.9%.

For comparison, the SNN results achieved above are benchmarked against the COCO mAP results achieved in [17] and are depicted in Figure 4. The authors in [17] trained their model on the Prophesee GEN1 dataset. It is observed that the SNNs trained on the NU-AIR dataset achieve mAP close to the mAP of the comparison study [17]. The COCO mAP of the VGG-11 + SSD model reached 0.17, and is the highest accuracy reported of the three trained models. However, [17] reported that DenseNet121-24 + SSD model achieved the highest accuracy in their work.

In terms of mAP, the VGG-11 + SSD and DenseNet121-16 configurations reported a higher object detection performance than the MobileNet-16 + SSD configuration. The DenseNet121-16 configuration achieved the mAP score with a smaller network and less accumulations than the VGG-11 architecture. This trade-off in performance may

be valuable on neuromorphic systems with constrained amounts of neurons. However, VGG-11 uses the most sparse network structure, which is best suited for use in power constrained embedded hardware.

The lower performance of the MobileNet architecture was observed to be related to the use of depth-wise separable convolutions. In [17], depth-wise separable convolutions were shown to reduce performance in smaller networks (less than 32 input channels) when compared to normal convolutions. Although depth-wise separable convolutions enable the use of a smaller number of network parameters, thus making the training of the SNN with surrogate gradients a simpler task, small networks were shown to benefit from the additional network size for a 5% increase in accuracy. Thus, a larger variant of MobileNet (larger than 16) may be used to yield an increase in network performance.

### 4.3 Ablation Study of Baseline SNNs

#### 4.3.1 Effect of Depth Variation on SNN Performance

The network’s architecture size can significantly impact the model’s performance. It’s often observed that larger networks perform better, mainly due to their enhanced capacity for learning complex representations [12, 93]. However, this increased performance often comes with a trade-off in terms of computational overhead and the risk of overfitting [97, 55]. This section presents results about the effect of changing the network size on SNN performance using variations of MobileNet, VGG, and DenseNet architectures. For each of the three baseline models (MobileNet-16, VGG-11, and DenseNet121-16), two additional networks were trained: a smaller (MobileNet-13, VGG-9, and DenseNet-98) and a larger (MobileNet-19, VGG-16, and DenseNet-142). The smaller networks had fewer layers and parameters than the baseline models, while the larger networks had more. Performance metrics of this ablation are presented in Figure 4.

The smaller MobileNet-13, VGG-9, and DenseNet-98 achieved a relative decrease in mAP of 7.69%, 5.88%, and 5.88%, respectively, compared to their baseline counterparts. This

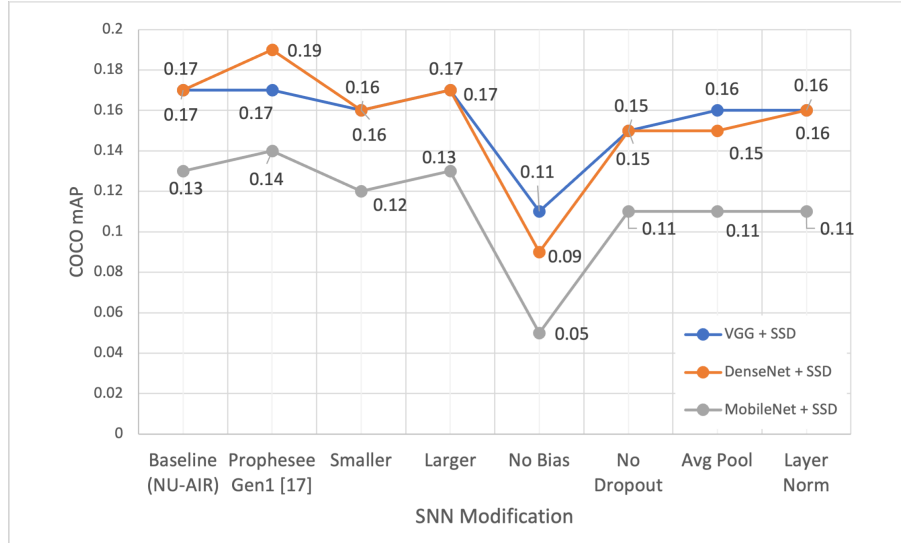


**Fig. 4** Comparison of the COCO mean average precision (mAP) for three spiking neural networks (SNNs) and their ablations trained on the presented dataset. The baseline results are compared to the performance of the Prophesee GEN1 dataset, as reported in [17]. The comparability between the collected data and the Prophesee Gen1 is anchored in the shared sensor modality, analogous dataset complexity, and benchmarking status of Prophesee GEN1.

performance reduction can be attributed to the decreased model capacity, leading to less effective extraction and representation of complex features in the input data. The larger network variations showed no gains over the baseline models, despite their additional capacity.

The larger networks came at the expense of substantially increased computational complexity and training time, bringing forth the question on cost-to-benefit. These results indicate overfitting risks, optimization difficulties due to deeper architectures, and lack of gains from additional capacity on a finite dataset.

#### 4.3.2 Effect of Bias Parameter Removal on SNN Performance

The bias parameter, usually initialized with a small constant or random value, has been recognized as a pivotal element in the structure of neural networks to provide an additional degree of freedom and enhance the ability of the network to generalize beyond the training data [25, 35]. This section presents an analysis of the consequences of removing bias parameters on the learning and subsequent network performance. The evaluation was performed by retraining the VGG-11, MobileNet-16, and DenseNet121-16 networks without bias parameters on the NU-AIR dataset. The removal

of bias parameters is performed by removing the bias initialization argument at each layer of these networks. The mAP performance of these models was subsequently compared with their conventional counterparts (i.e., with bias parameters intact). Figure 4 depicts the bias-free training results.

Specifically, for VGG, the baseline mAP was 0.17, which decreased to 0.11 when trained without bias. For DenseNet, the mAP dropped from a baseline of 0.17 to 0.09 upon bias removal. Similarly, MobileNet experienced a decline from 0.13 to 0.05 when the bias parameters were removed. The experimental results demonstrate a notable decrease in accuracy upon the removal of bias parameters from the VGG-11, MobileNet-16, and DenseNet121-16 networks. Such performance degradation is not unexpected. The bias parameters fundamentally serve to shift the activation function, assisting the learning process by introducing an additional degree of freedom that allows for a better fit to the training data. Bias removal, therefore, is akin to constraining the model’s capacity to learn intricate data distributions. Without bias parameters, the resulting linear transformations (imposed by weights alone) lack the necessary flexibility to adequately model

the non-linear decision boundaries present in high-dimensional data spaces, such as those of the NU-AIR dataset. Consequently, the effective learning capacity of the network diminishes, leading to a drop in mAP performance.

#### 4.3.3 Effect of Dropout Layers Removal on SNN Performance

Dropout is a common regularization technique used to reduce overfitting by deactivating a subset of neurons during training [97]. The result is that the network creates more robust internal representations and reduces the model's reliance on specific feature pathways [5]. This section presents an analysis of the impact of using Dropout compared to its absence in the VGG-11, MobileNet-16, and DenseNet121 architectures. A variant of each model was trained on the dataset with all Dropout layers removed.

The mAP performance of these Dropout-exclusive models was compared with the Dropout-inclusive models trained according to Section 4.2. Figure 4 depicts the Dropout-exclusive training results. The results demonstrate that the removal of Dropout resulted in a reduction in the mAP for the three models. Specifically, the mAP for VGG-11 decreased from 0.17 to 0.16, MobileNet-16 from 0.13 to 0.11, and DenseNet121 from 0.19 to 0.16. The observed reduction in mAP is consistent with the function of Dropout as a regularization technique. Without Dropout, networks are more susceptible to overfitting, particularly in the context of high-dimensional datasets such as NU-AIR. The resulting models are unable to generalize effectively to unseen data, thus leading to a decrease in test set mAP performance. The results highlight the importance of Dropout in striking a balance between model complexity and generalizability, ultimately leading to better performance on the real world data.

#### 4.3.4 Effect of Average Pooling Layers on SNN Performance

Pooling layers are fundamental to CNNs and SNNs, providing translation invariance and reducing computational complexity by downsampling the feature maps [90, 99]. Max Pooling and Average Pooling are two commonly used strategies for spatial downsampling in SNNs [69, 36]. This section presents a comparative analysis of the

two pooling strategies, focusing on their effect on mAP performance of VGG-11, MobileNet-16, and DenseNet121 networks trained on the NU-AIR dataset. Each network was trained under two distinct configurations: one with Max Pooling layers (baseline configuration), and another with Average Pooling Layers. The results are depicted in Figure 4.

The evaluation results depict a notable difference in performance across the two configurations. For VGG-11, replacing Max Pooling layers with Average Pooling resulted in a decline of 5.88% in the mAP. This decrement was more pronounced for the MobileNet-16 and DenseNet121 networks, which saw a drop of 15.38% and 11.76%, respectively.

These results indicate a clear preference for Max Pooling over Average Pooling in the context of the NU-AIR dataset and these specific SNN architectures. This drop in performance can be attributed to the fact that while Max Pooling captures the most dominant feature in a particular region, Average Pooling computes the mean of the features which may lead to a loss of critical discriminative information.

#### 4.3.5 Effect of Batch Normalization vs Layer Normalization on SNN Performance

Normalization techniques stabilize and accelerate the learning process by regulating network inputs along either the batch [48, 8, 89] or feature dimensions [4]. This section provides discusses the effect of replacing BatchNorm with LayerNorm in VGG-11, MobileNet-16, and DenseNet121 architectures trained on the NU-AIR dataset. These networks were trained with two distinct configurations: one with BatchNorm (baseline configuration), and the other with LayerNorm. The comparative analysis was carried out using the mAP metric. The results are shown in Figure 4.

The comparative analysis revealed a performance difference across the two configurations. For the DenseNet121 and VGG-11 architectures, replacing BatchNorm with LayerNorm led to decreases of 5.88% in mAP. The difference was more pronounced in the MobileNet-16 network, which experienced a drop in mAP of 15.38%.

These results can be attributed to the core differences between BatchNorm and LayerNorm.

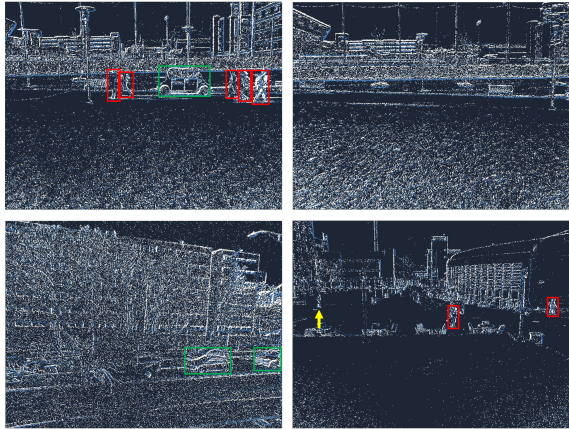


**Fig. 5** Success and failure cases of the detection method on NU-AIR depicted, clockwise from top left: True Positive: Successful detection of vehicles and pedestrians; True Negative: Correct absence of detections; False Negative: Missed detection of a pedestrian (indicated by yellow arrow); False Positive: Two vehicles inaccurately identified as a single vehicle.

BatchNorm normalizes across the batch dimension, thus leveraging batch statistics to maintain a stable distribution of activations. BatchNorm also provides implicit regularization by introducing noise to the training process. This noise is created by fluctuations of the mean and variance of the preceding layer activations across different batches. On the contrary, LayerNorm normalizes over the feature dimension, thus maintaining a consistent activation distribution within each individual sample. LayerNorm computes normalized statistics from individual samples, reducing the inherent noise as well as the model’s ability to generalize beyond the training data, as reflected in the lower mAP results.

## 5 Limitations

Some limitations of the presented work are discussed here.

1. The SNNs evaluated in this study were trained and evaluated on GPU hardware, which differs from the low-power neuromorphic hardware that is the intended target for this type of application. Therefore, the reported performance may not be representative of how these models would perform in real-world edge devices. The recently released Intel Loihi 2 could be used

to further enhance the dataset benchmarking experiments and results [74].

2. The DNNs evaluated in this study were trained on frame-based grey-scale images and did not leverage color information or the temporal information of spikes. This limited approach may have negatively impacted the object detection performance of these models.
3. The data used to train and evaluate the models was collected from a single city in New Jersey, which may limit the generalizability of the reported results to other settings. Future work should evaluate the performance of these models using data collected from multiple urban settings to assess the generalizability of the models.
4. Aerial data acquisition through drones inherently grapples with specific drone-induced artifacts that perturb the optical fidelity of the captured sequences [91]. These artifacts, stemming from intricate drone kinematics and atmospheric interferences, imprint stochastic translational and rotational perturbations onto the footage, manifesting as jitter, inadvertent panning, and axis misalignment [65, 1]. These spatiotemporal incongruities disrupt the optical flow coherence, infusing the sequences with undesirable optical phenomena like motion-induced blur, consecutive frame misregistration, and depth-induced parallax anomalies. Such aberrations invariably compromise the optical clarity and spatial resolution of the sequences. Figure 5 depicts examples of successful and unsuccessful visualizations of various detection cases. The network’s responses to these detection cases are influenced by the inherent challenges associated with differentiating between objects and background noise, and handling occlusions within the given data. For the false negative case, the pedestrian, due to their relatively smaller size, has been incorrectly classified as part of the background. This is a common challenge in object detection, especially in complex urban environments where numerous similar-sized non-target objects, such as lampposts or trash bins, are present. The detector’s sensitivity towards small objects can be adversely affected by this, leading to the missed detection seen. In the false positive case, two vehicles are closely aligned and incorrectly detected as a single

target. This issue arises when dealing with real-world scenarios where objects often overlap or occlude one another. With uncertain boundary information between closely located or overlapping objects, the network may perceive these objects as a single entity, leading to false positives.

## 6 Conclusion

A neuromorphic quadrotor-based dataset for pedestrian/vehicle detection and localization in urban environments was presented. The dataset has been fully annotated and is open sourced along with all accompanying Python code for the community. The dataset was used to train VGG, MobileNet, and DenseNet SNNs to evaluate object detection and localization tasks through a comprehensive ablation study. Ten frame-based single- and two-stage object detector DNNs were also used to evaluate the mAP of the dataset on object detection tasks. The experimental accuracy results of SNNs were on-par with results observed with matching networks trained on other large scale, contemporary datasets underscoring the reliability of the presented data. Object detection, notwithstanding its pervasive nature in the domain, stands as both a foundational and non-trivial task in computer vision [109]. In light of this, the presented dataset accentuates the potential pitfalls arising from drone-related visual anomalies and such motion-induced blurring, jitter-related frame misalignments, and nuanced scale and perspective shifts. Concurrently, the onus on algorithmic methodologies is to proficiently handle the pronounced sparsity and refined temporal dynamics inherent to event-driven visual data. Future work will extend this study to perform instance and semantic segmentation on a wider variety of urban scenes.

## References

- [1] Aguilar WG, Angulo C (2016) Real-time model-based video stabilization for microaerial vehicles. *Neural processing letters* 43:459–477
- [2] Amir A, Taba B, Berg DJ, et al (2017) A low power, fully event-based gesture recognition system. 2017 IEEE Conference on Computer Vision and Pattern Recognition (CVPR) pp 7388–7397
- [3] Anderson K, Gaston KJ (2013) Lightweight unmanned aerial vehicles will revolutionize spatial ecology. *Frontiers in Ecology and the Environment* 11(3):138–146
- [4] Ba JL, Kiros JR, Hinton GE (2016) Layer normalization. arXiv preprint arXiv:160706450
- [5] Baldi P, Sadowski PJ (2013) Understanding dropout. *Advances in neural information processing systems* 26
- [6] Bardow P, Davison AJ, Leutenegger S (2016) Simultaneous optical flow and intensity estimation from an event camera. In: *Proceedings of the IEEE conference on computer vision and pattern recognition*, pp 884–892
- [7] Barnas AF, Darby BJ, Vandeberg GS, et al (2019) A comparison of drone imagery and ground-based methods for estimating the extent of habitat destruction by lesser snow geese (*anser caerulescens caerulescens*) in la pérouse bay. *PLoS One* 14(8):e0217049
- [8] Bjorck N, Gomes CP, Selman B, et al (2018) Understanding batch normalization. *Advances in neural information processing systems* 31
- [9] Bock J, Krajewski R, Moers T, et al (2020) The ind dataset: A drone dataset of naturalistic road user trajectories at german intersections. In: *2020 IEEE Intelligent Vehicles Symposium (IV)*, IEEE, pp 1929–1934
- [10] Braun M, Krebs S, Flohr F, et al (2019) Eurocity persons: A novel benchmark for person detection in traffic scenes. *IEEE transactions on pattern analysis and machine intelligence* 41(8):1844–1861
- [11] Breuer A, Termöhlen JA, Homoceanu S, et al (2020) opendd: A large-scale roundabout drone dataset. In: *2020 IEEE 23rd International Conference on Intelligent Transportation Systems (ITSC)*, IEEE, pp

- [12] Brutzkus A, Globerson A (2019) Why do larger models generalize better? a theoretical perspective via the xor problem. In: International Conference on Machine Learning, PMLR, pp 822–830
- [13] del Cerro J, Cruz Ulloa C, Barrientos A, et al (2021) Unmanned aerial vehicles in agriculture: A survey. *Agronomy* 11(2):203
- [14] Chen S, Akselrod P, Zhao B, et al (2012) Efficient feedforward categorization of objects and human postures with address-event image sensors. *IEEE Transactions on Pattern Analysis and Machine Intelligence* 34(2):302–314. <https://doi.org/10.1109/TPAMI.2011.120>
- [15] Chen Y, Wang Y, Lu P, et al (2018) Large-scale structure from motion with semantic constraints of aerial images. In: Chinese Conference on Pattern Recognition and Computer Vision (PRCV), Springer, pp 347–359
- [16] Cordone L, Miramond B, Ferrante S (2021) Learning from event cameras with sparse spiking convolutional neural networks. In: 2021 International Joint Conference on Neural Networks (IJCNN), IEEE, pp 1–8
- [17] Cordone L, Miramond B, Thierion P (2022) Object detection with spiking neural networks on automotive event data. In: Proceedings of the IEEE International Joint Conference on Neural Networks (IJCNN)
- [18] Daknama R, Kraus E (2017) Vehicle routing with drones. arXiv preprint arXiv:170506431
- [19] Dalal N, Triggs B (2005) Histograms of oriented gradients for human detection. In: 2005 IEEE computer society conference on computer vision and pattern recognition (CVPR'05), Ieee, pp 886–893
- [20] De Tournemire P, Nitti D, Perot E, et al (2020) A large scale event-based detection dataset for automotive. arXiv preprint arXiv:200108499
- [21] Dilshad N, Hwang J, Song J, et al (2020) Applications and challenges in video surveillance via drone: A brief survey. In: 2020 International Conference on Information and Communication Technology Convergence (ICTC), IEEE, pp 728–732
- [22] DJI (2022) Dji matrice m100: Quadcopter for developers. <https://www.dji.com/matrice100>
- [23] DJI (2022) Matrice 100 tb48d battery. <https://store.dji.com/product/matrice-100-tb48d-battery>
- [24] Dollár P, Wojek C, Schiele B, et al (2009) Pedestrian detection: A benchmark. In: 2009 IEEE conference on computer vision and pattern recognition, IEEE, pp 304–311
- [25] Dongare A, Kharde R, Kachare AD, et al (2012) Introduction to artificial neural network. *International Journal of Engineering and Innovative Technology (IJEIT)* 2(1):189–194
- [26] Du D, Qi Y, Yu H, et al (2018) The unmanned aerial vehicle benchmark: Object detection and tracking. In: Proceedings of the European conference on computer vision (ECCV), pp 370–386
- [27] Enzweiler M, Gavrila DM (2008) Monocular pedestrian detection: Survey and experiments. *IEEE transactions on pattern analysis and machine intelligence* 31(12):2179–2195
- [28] Escobar MJ, Masson GS, Viéville T, et al (2009) Action recognition using a bio-inspired feedforward spiking network. *International Journal of Computer Vision* 82:284–301. URL <https://api.semanticscholar.org/CorpusID:441561>
- [29] Ess A, Leibe B, Schindler K, et al (2008) A mobile vision system for robust multi-person tracking. In: 2008 IEEE Conference

- on Computer Vision and Pattern Recognition, IEEE, pp 1–8
- [30] Fang W, Yu Z, Chen Y, et al (2021) Incorporating learnable membrane time constant to enhance learning of spiking neural networks. In: Proceedings of the IEEE/CVF International Conference on Computer Vision, pp 2661–2671
- [31] Fei-Fei L, Fergus R, Perona P (2004) Learning generative visual models from few training examples: An incremental bayesian approach tested on 101 object categories. Computer Vision and Pattern Recognition Workshop
- [32] Fromm M, Schubert M, Castilla G, et al (2019) Automated detection of conifer seedlings in drone imagery using convolutional neural networks. *Remote Sensing* 11(21):2585
- [33] Gallego G, Delbrück T, Orchard G, et al (2020) Event-based vision: A survey. *IEEE transactions on pattern analysis and machine intelligence* 44(1):154–180
- [34] Geiger A, Lenz P, Stiller C, et al (2013) Vision meets robotics: The kitti dataset. *The International Journal of Robotics Research* 32(11):1231–1237
- [35] Geman S, Bienenstock E, Doursat R (1992) Neural networks and the bias/variance dilemma. *Neural computation* 4(1):1–58
- [36] Gholamalinezhad H, Khosravi H (2020) Pooling methods in deep neural networks, a review. arXiv preprint arXiv:200907485
- [37] Google (2023) Colaboratory: Frequently asked questions. <https://research.google.com/colaboratory/faq.html>
- [38] Google (2023) Google cloud compute platform. <https://console.cloud.google.com>
- [39] Guerrero-Gómez-Olmedo R, Torre-Jiménez B, López-Sastre R, et al (2015) Extremely overlapping vehicle counting. In: Pattern Recognition and Image Analysis: 7th Iberian Conference, IbPRIA 2015, Santiago de Compostela, Spain, June 17-19, 2015, Proceedings 7, Springer, pp 423–431
- [40] Gupta H, Verma OP (2022) Monitoring and surveillance of urban road traffic using low altitude drone images: a deep learning approach. *Multimedia Tools and Applications* pp 1–21
- [41] Harris CR, Millman KJ, van der Walt SJ, et al (2020) Array programming with NumPy. *Nature* 585(7825):357–362. <https://doi.org/10.1038/s41586-020-2649-2>, URL <https://doi.org/10.1038/s41586-020-2649-2>
- [42] Hirano Y, Garcia C, Sukthankar R, et al (2006) Industry and object recognition: Applications, applied research and challenges. In: *Toward category-level object recognition*. Springer, p 49–64
- [43] Hossain S, Lee Dj (2019) Deep learning-based real-time multiple-object detection and tracking from aerial imagery via a flying robot with gpu-based embedded devices. *Sensors* 19(15):3371
- [44] Howard AG, Zhu M, Chen B, et al (2017) Mobilenets: Efficient convolutional neural networks for mobile vision applications. arXiv preprint arXiv:170404861
- [45] Huang G, Liu Z, Van Der Maaten L, et al (2017) Densely connected convolutional networks. In: Proceedings of the IEEE conference on computer vision and pattern recognition, pp 4700–4708
- [46] Iaboni C, Patel H, Lobo D, et al (2021) Event camera based real-time detection and tracking of indoor ground robots. *IEEE Access* 9:166588–166602
- [47] Iaboni C, Lobo D, Choi JW, et al (2022) Event-based motion capture system for online multi-quadrotor localization and tracking. *Sensors* 22(9):3240
- [48] Ioffe S, Szegedy C (2015) Batch normalization: Accelerating deep network training by

- reducing internal covariate shift. In: International conference on machine learning, pmlr, pp 448–456
- [49] Jocher G, Chaurasia A, Qiu J (2023) YOLO by Ultralytics. URL <https://github.com/ultralytics/ultralytics>
- [50] Jocher G, et al (2020) ultralytics/yolov5. <https://doi.org/10.5281/zenodo.4154370>, URL <https://doi.org/10.5281/zenodo.4154370>
- [51] Joyce K, Duce S, Leahy S, et al (2018) Principles and practice of acquiring drone-based image data in marine environments. *Marine and Freshwater Research* 70(7):952–963
- [52] Kim S, Park S, Na B, et al (2019) Spiking-yolo: Spiking neural network for energy-efficient object detection. [1903.06530](https://arxiv.org/abs/1903.06530)
- [53] Koch S, Weber T, Sobottka C, et al (2016) Outdoor electroluminescence imaging of crystalline photovoltaic modules: Comparative study between manual ground-level inspections and drone-based aerial surveys. In: 32nd European Photovoltaic Solar Energy Conference and Exhibition, pp 1736–1740
- [54] Kugele A, Pfeil T, Pfeiffer M, et al (2020) Efficient processing of spatio-temporal data streams with spiking neural networks. *Frontiers in Neuroscience* 14:439
- [55] Lawrence S, Giles CL (2000) Overfitting and neural networks: conjugate gradient and backpropagation. In: Proceedings of the IEEE-INNS-ENNS International Joint Conference on Neural Networks. IJCNN 2000. Neural Computing: New Challenges and Perspectives for the New Millennium, IEEE, pp 114–119
- [56] Li C, Li L, Jiang H, et al (2022) Yolov6: A single-stage object detection framework for industrial applications. arXiv preprint arXiv:220902976
- [57] Li H, Liu H, Ji X, et al (2017) Cifar10-dvs: An event-stream dataset for object classification. *Frontiers in Neuroscience* 11. <https://doi.org/10.3389/fnins.2017.00309>, URL <https://www.frontiersin.org/article/10.3389/fnins.2017.00309>
- [58] Liang M, Delahaye D (2019) Drone fleet deployment strategy for large scale agriculture and forestry surveying. In: 2019 IEEE Intelligent Transportation Systems Conference (ITSC), IEEE, pp 4495–4500
- [59] Lin TY, Maire M, Belongie S, et al (2014) Microsoft coco: Common objects in context. In: Computer Vision–ECCV 2014: 13th European Conference, Zurich, Switzerland, September 6–12, 2014, Proceedings, Part V 13, Springer, pp 740–755
- [60] Lin TY, Goyal P, Girshick R, et al (2017) Focal loss for dense object detection. In: Proceedings of the IEEE international conference on computer vision, pp 2980–2988
- [61] Liu W, Anguelov D, Erhan D, et al (2016) Ssd: Single shot multibox detector. In: Computer Vision–ECCV 2016: 14th European Conference, Amsterdam, The Netherlands, October 11–14, 2016, Proceedings, Part I 14, Springer, pp 21–37
- [62] Loshchilov I, Hutter F (2019) Decoupled weight decay regularization. [1711.05101](https://arxiv.org/abs/1711.05101)
- [63] Marathe S (2019) Leveraging drone based imaging technology for pipeline and road monitoring survey. In: SPE Asia Pacific Health, Safety, Security, Environment and Social Responsibility Symposium?, SPE, p D021S006R001
- [64] Miao S, Chen G, Ning X, et al (2019) Neuromorphic benchmark datasets for pedestrian detection, action recognition, and fall detection. *Frontiers in neurorobotics* 13:38
- [65] Mingkhwan E, Khawsuk W (2017) Digital image stabilization technique for fixed camera on small size drone. In: 2017 Third Asian Conference on Defence Technology (ACDT), IEEE, pp 12–19

- [66] Mittal P, Singh R, Sharma A (2020) Deep learning-based object detection in low-altitude uav datasets: A survey. *Image and Vision computing* 104:104046
- [67] Moeys DP, Neil D, Corradi F, et al (2018) Pred18: Dataset and further experiments with davis event camera in predator-prey robot chasing. *IEEE Fourth International Conference on Event-Based Control, Communication and Signal Processing (EBCCSP) 2018* <https://doi.org/10.48550/ARXIV.1807.03128>, URL <https://arxiv.org/abs/1807.03128>
- [68] Mueller M, Smith N, Ghanem B (2016) A benchmark and simulator for uav tracking. In: *Computer Vision–ECCV 2016: 14th European Conference, Amsterdam, The Netherlands, October 11–14, 2016, Proceedings, Part I* 14, Springer, pp 445–461
- [69] Nagi J, Ducatelle F, Di Caro GA, et al (2011) Max-pooling convolutional neural networks for vision-based hand gesture recognition. In: *2011 IEEE international conference on signal and image processing applications (ICSIPA)*, IEEE, pp 342–347
- [70] Negri P, Soto M, Linares-Barranco B, et al (2018) Scene context classification with event-driven spiking deep neural networks. In: *2018 25th IEEE International Conference on Electronics, Circuits and Systems (ICECS)*, pp 569–572, <https://doi.org/10.1109/ICECS.2018.8617982>
- [71] Negri P, Soto M, Linares-Barranco B, et al (2018) Scene context classification with event-driven spiking deep neural networks. In: *2018 25th IEEE International Conference on Electronics, Circuits and Systems (ICECS)*, IEEE, pp 569–572
- [72] Nvidia (2022) Nvidia jetson agx xavier development kit. <https://www.nvidia.com/en-us/autonomous-machines/embedded-systems/jetson-agx-xavier/>
- [73] Orchard G, Jayawant A, Cohen GK, et al (2015) Converting static image datasets to spiking neuromorphic datasets using saccades. *Frontiers in Neuroscience* 9. <https://doi.org/10.3389/fnins.2015.00437>, URL <https://www.frontiersin.org/article/10.3389/fnins.2015.00437>
- [74] Orchard G, Frady EP, Rubin DBD, et al (2021) Efficient neuromorphic signal processing with loihi 2. In: *2021 IEEE Workshop on Signal Processing Systems (SiPS)*, IEEE, pp 254–259
- [75] Pang Y, Cao J, Li Y, et al (2020) Tju-dhd: A diverse high-resolution dataset for object detection. *IEEE Transactions on Image Processing* 30:207–219
- [76] Papadopoulos DP, Uijlings JR, Keller F, et al (2017) Extreme clicking for efficient object annotation. In: *Proceedings of the IEEE international conference on computer vision*, pp 4930–4939
- [77] Perot E, De Tournemire P, Nitti D, et al (2020) Learning to detect objects with a 1 megapixel event camera. *Advances in Neural Information Processing Systems* 33:16639–16652
- [78] Prophesee (2022) Prophesee evk1 - gen3.1 vga. <https://docs.prophesee.ai/stable/hw/evk/gen3.html>
- [79] Puri A (2005) A survey of unmanned aerial vehicles (uav) for traffic surveillance. *Department of computer science and engineering, University of South Florida* pp 1–29
- [80] Pérez-Carrasco J, Zhao B, Serrano C, et al (2013) Mapping from frame-driven to frame-free event-driven vision systems by low-rate rate-coding and coincidence processing. application to feed forward convnets. *IEEE Transactions on Pattern Analysis and Machine Intelligence* 35:2706 – 2719. <https://doi.org/10.1109/TPAMI.2013.71>
- [81] Ramachandran A, Sangaiah AK (2021) A review on object detection in unmanned aerial vehicle surveillance. *International Journal of Cognitive Computing in Engineering* 2:215–228

- [82] Rebecq H, Gallego G, Mueggler E, et al (2018) Emvs: Event-based multi-view stereo—3d reconstruction with an event camera in real-time. *International Journal of Computer Vision* 126. <https://doi.org/10.1007/s11263-017-1050-6>
- [83] Reckling W, Mitasova H, Wegmann K, et al (2021) Efficient drone-based rare plant monitoring using a species distribution model and ai-based object detection. *Drones* 5(4):110
- [84] Ren S, He K, Girshick R, et al (2015) Faster r-cnn: Towards real-time object detection with region proposal networks. *Advances in neural information processing systems* 28
- [85] Roldán-Gómez JJ, González-Gironda E, Barrientos A (2021) A survey on robotic technologies for forest firefighting: Applying drone swarms to improve firefighters' efficiency and safety. *Applied Sciences* 11(1):363
- [86] Russakovsky O, Deng J, Su H, et al (2015) Imagenet large scale visual recognition challenge. *International journal of computer vision* 115:211–252
- [87] Sandino J, Vanegas F, Maire F, et al (2020) Uav framework for autonomous onboard navigation and people/object detection in cluttered indoor environments. *Remote Sensing* 12(20):3386
- [88] Sandino J, Maire F, Caccetta P, et al (2021) Drone-based autonomous motion planning system for outdoor environments under object detection uncertainty. *Remote Sensing* 13(21):4481
- [89] Santurkar S, Tsipras D, Ilyas A, et al (2018) How does batch normalization help optimization? *Advances in neural information processing systems* 31
- [90] Scherer D, Müller A, Behnke S (2010) Evaluation of pooling operations in convolutional architectures for object recognition. In: *International conference on artificial neural networks*, Springer, pp 92–101
- [91] Seifert E, Seifert S, Vogt H, et al (2019) Influence of drone altitude, image overlap, and optical sensor resolution on multi-view reconstruction of forest images. *Remote sensing* 11(10):1252
- [92] Serrano-Gotarredona T, Linares-Barranco B (2013) A 128x128 1.5% contrast sensitivity 0.9% fpn 3  $\mu$ s latency 4 mw asynchronous frame-free dynamic vision sensor using transimpedance preamplifiers. *IEEE Journal of Solid-State Circuits* 48(3):827–838. <https://doi.org/10.1109/JSSC.2012.2230553>
- [93] Shazeer N, Mirhoseini A, Maziarz K, et al (2017) Outrageously large neural networks: The sparsely-gated mixture-of-experts layer. *arXiv preprint arXiv:170106538*
- [94] Shi X, Chen Z, Wang H, et al (2015) Convolutional lstm network: A machine learning approach for precipitation nowcasting. *Advances in neural information processing systems* 28
- [95] Simonyan K, Zisserman A (2014) Very deep convolutional networks for large-scale image recognition. *arXiv preprint arXiv:14091556*
- [96] Sironi A, Brambilla M, Bourdis N, et al (2018) Hats: Histograms of averaged time surfaces for robust event-based object classification. In: *Proceedings of the IEEE conference on computer vision and pattern recognition*, pp 1731–1740
- [97] Srivastava N, Hinton G, Krizhevsky A, et al (2014) Dropout: a simple way to prevent neural networks from overfitting. *The journal of machine learning research* 15(1):1929–1958
- [98] Su H, Deng J, Fei-Fei L (2012) Crowdsourcing annotations for visual object detection. In: *Workshops at the twenty-sixth AAAI conference on artificial intelligence*, Citeseer
- [99] Sun M, Song Z, Jiang X, et al (2017) Learning pooling for convolutional neural network. *Neurocomputing* 224:96–104

- [100] Varghese A, Gubbi J, Sharma H, et al (2017) Power infrastructure monitoring and damage detection using drone captured images. In: 2017 international joint conference on neural networks (IJCNN), IEEE, pp 1681–1687
- [101] Vasudevan A, Negri P, Linares-Barranco B, et al (2020) Introduction and analysis of an event-based sign language dataset. In: 2020 15th IEEE International Conference on Automatic Face and Gesture Recognition (FG 2020), <https://doi.org/10.1109/FG47880.2020.00069>
- [102] Wang CY, Bochkovskiy A, Liao HYM (2022) Yolov7: Trainable bag-of-freebies sets new state-of-the-art for real-time object detectors. arXiv preprint arXiv:220702696
- [103] Wen L, Du D, Cai Z, et al (2020) Uadetrac: A new benchmark and protocol for multi-object detection and tracking. Computer Vision and Image Understanding 193:102907
- [104] Wojek C, Walk S, Schiele B (2009) Multi-cue onboard pedestrian detection. In: 2009 IEEE Conference on Computer Vision and Pattern Recognition, IEEE, pp 794–801
- [105] Zhang S, Benenson R, Schiele B (2017) Citypersons: A diverse dataset for pedestrian detection. In: Proceedings of the IEEE conference on computer vision and pattern recognition, pp 3213–3221
- [106] Zheng L, Zhang H, Sun S, et al (2017) Person re-identification in the wild. In: Proceedings of the IEEE conference on computer vision and pattern recognition, pp 1367–1376
- [107] Zhilenkov AA, Epifantsev IR (2018) System of autonomous navigation of the drone in difficult conditions of the forest trails. In: 2018 IEEE Conference of Russian Young Researchers in Electrical and Electronic Engineering (EICoRus), IEEE, pp 1036–1039
- [108] Zhu P, Wen L, Du D, et al (2021) Detection and tracking meet drones challenge. IEEE Transactions on Pattern Analysis and Machine Intelligence pp 1–1. <https://doi.org/10.1109/TPAMI.2021.3119563>
- [109] Zou Z, Chen K, Shi Z, et al (2023) Object detection in 20 years: A survey. Proceedings of the IEEE